Phase behaviour of symmetric binary mixtures with partially miscible components in slit-like pores. Application of the fundamental measure density functional approach

2003 J. Phys.: Condens. Matter 15 2269

(http://iopscience.iop.org/0953-8984/15/14/303)

INSTITUTE OF PHYSICS PUBLISHING JOURNAL OF PHYSICS: CONDENSED MATTER

J. Phys.: Condens. Matter **15** (2003) 2269–2283 PII: S0953-8984(03)56412-8

Phase behaviour of symmetric binary mixtures with partially miscible components in slit-like pores. Application of the fundamental measure density functional approach

Arturo Martinez[1], **Orest Pizio**[2], **Andrzej Patrykiejew**[3] **and Stefan Sokołowski**[3]

[1] Facultad de Quimica, UNAM, Mexico, DF, Mexico
[2] Instituto de Quimica, UNAM, Circuito Exterior, Coyoacan 04510, Mexico, DF, Mexico
[3] Department for the Modelling of Physico-Chemical Processes, Maria Curie-Skłodowska University, 20031 Lublin, Poland

E-mail: pizio@servidor.unam.mx

Received 20 November 2002, in final form 24 February 2003
Published 31 March 2003
Online at stacks.iop.org/JPhysCM/15/2269

Abstract

We investigate adsorption in slit-like pores of model symmetric binary mixtures exhibiting demixing in bulk phase, by using a density functional approach. Our focus is on the evaluation of the first-order phase transitions in adsorbed fluids and the lines separating mixed and demixed phases. The scenario for phase transitions is sensitive to the pore width and to the energy of adsorption. Both these parameters can change the phase diagrams of the confined fluid. In particular, for relatively wide pores and for strong wall–fluid interactions, the demixing line can precede the first-order transition. Moreover, a competition between layering transitions and demixing within particular layers also leads to further enrichment of the phase diagram.

1. Introduction

Single-component fluids confined to micropores can exhibit several types of phase behaviour, due to the competition between fluid–solid and fluid–fluid interactions, see e.g. [1]. In particular, the first-order surface phase transitions, such as prewetting and layering, can be observed in such systems. These phenomena do not have their counterparts in the bulk fluids. On the other hand, in the case of the usual phase transitions such as condensation and freezing, the confinement causes shifts of their characteristic parameters and the coexistence lines.

Principal theoretical issues concerning phase transitions in confined fluids are to understand basic physical phenomena and to determine how the transitions are affected by the pore geometry and size, by the fluid–pore walls interactions and by the state conditions of an adsorbate. In addition to solely academic interest, knowledge of the physical chemistry of

phase transformations is of much importance for applied research. In fact, the investigation of adsorption of fluid mixtures is more important than of single-component fluids and the number of theoretical and simulational works dedicated to that problem is very large and growing, cf [2–16].

Description of phase behaviour of *bulk* fluid mixtures [17–22], in spite of certain advances, still remains incomplete in several aspects. Although several possible phase diagram topologies have been placed into a number of categories [20–22], the knowledge (even within mean-field type approaches) which microscopic features are responsible for yielding a given category is far from being satisfactory. The confinement of a fluid must lead to further complications. Consequently, theoretical description of phase behaviour of confined binary mixtures remains at its preliminary stage.

The aim of the present study is to present such a description within the framework of a density functional approach. We use a simple model of a binary mixture. This model is known in the literature as the so-called symmetric binary mixture model [14, 20, 21, 23]. This model includes two species, $i = 1, 2$, of equal diameters, $\sigma_1 = \sigma_2 = \sigma$ (thus it ignores the influence of the size ratio on the phase behaviour). Additivity of diameters is assumed, $\sigma_{12} = 0.5(\sigma_1+\sigma_2) = \sigma$. The interactions between like particles are chosen equal, with identical functional form (e.g. Lennard-Jones (LJ) potential) and are characterized by the same energy parameters, $\varepsilon_{11} = \varepsilon_{22} = \varepsilon$. The 'cross' interaction potential between unlike particles also has the same functional form and is characterized by the energy parameter $\varepsilon_{12} < \varepsilon$. The reduction of the number of parameters permits transparent interpretation of the results, and allows for establishing clear links between microscopic quantities and the resulting phase behaviour. We also assume that pore walls are energetically uniform, i.e. the pore walls–fluid particle potentials depend only on the distance normal to the wall, z. For simplicity and in order to reduce the number of parameters to a minimum, the fluid–solid potentials are chosen independent of adsorbate species.

In spite of its apparent simplicity, *homogeneous* binary symmetric mixtures exhibit quite interesting thermodynamic behaviour. Of particular importance is the modification of the coexistence curve for the first-order gas–liquid phase transition by the occurrence of the second-order demixing transition. If the value of the ratio $\varepsilon_{12}/\varepsilon$ changes, then an interesting and nontrivial interplay between the transitions can take place. Wilding *et al* [21] have proposed a classification scheme consisting of three types of topology of the phase diagram for such a simple binary mixture.

It is not known at present how and to what extent each of the types of bulk phase diagrams is affected by the confinement. The principal objective of our work is to consider that problem. We shall investigate the phase behaviour of a set of model fluids, confined in slit-like pores. Those fluids exhibit different demixing in a bulk system. The results obtained here permit us to discuss general trends and to classify topologies of the phase diagrams for *inhomogeneous* binary symmetric mixtures. Undoubtedly, our conclusions on many aspects should remain valid for cylindrical pores as well. On the other hand, they can serve as an useful benchmark for further investigations of more sophisticated models with several types of confining walls.

2. The models and theory

The system in question is a two-component fluid of spherical particles of species 1 and 2 interacting via the LJ potential [14, 20, 21, 23], truncated for technical reasons:

$$u_{ij}(r) = \begin{cases} u_{ij}^{LJ}(r), & r < r_{ij,cut} \\ 0, & r \geqslant r_{ij,cut}, \end{cases} \tag{1}$$

$$u_{ij}^{LJ}(r) = 4\varepsilon_{ij}\left[\left(\frac{\sigma_{ij}}{r}\right)^{12} - \left(\frac{\sigma_{ij}}{r}\right)^{6}\right], \tag{2}$$

where $r_{ij,cut}$ is the cut-off distance. We would like to introduce reduced units from the very beginning. Throughout this work the parameters σ and ε are chosen as the units of length and energy, respectively. Then, the reduced temperature is defined as usual, $T^* = kT/\varepsilon$. In all our calculations the cut-off distance was the same for all the components, $r_{ij,cut}/\sigma = 2.5$.

The choice of the value of the energy parameter for the LJ potential between unlike particles, $\varepsilon_{12}/\varepsilon$, is crucial. In this work we study three types of models with $\varepsilon_{12}/\varepsilon = 0.75$, 0.65 and 0.55. The models are abbreviated as M75, M65 and M55, for the sake of convenience. In the bulk these models yield three types of phase diagrams described below.

The fluid is confined in a slit-like pore of the width H. Both pore walls, $\alpha = 1, 2$, are identical and are characterized by the same potentials, $v(z)$, acting on particles of both species:

$$v(z) = \varepsilon_{gs}[(z_0/z)^9 - (z_0/z)^3]. \tag{3}$$

The total gas-pore potential is the sum of the contributions (3) due to two planar walls, located at $z = 0$ and H, such that $V(z) = v(z) + v(H - z)$. Without loss of generality, we have chosen $z_0/\sigma = 0.5$ for both components. The parameter ε_{gs}, in what follows, is measured in ε units. The model for the adsorption potential is an idealization, in comparison to real solid surfaces. However, the principal focus of our work is to reveal some general trends of the phase behaviour of the confined mixture rather than to deal with specific solid substrates. According to this objective, the number of model parameters has been reduced to a minimum, as has been mentioned above.

The local densities, $\rho_i(z)$, of the species $i = 1, 2$ are computed according to a density functional approach. In the present study we use the fundamental measure density functional method, originally derived by Rosenfeld [31], which is known as one of the most accurate to describe nonuniform fluid mixtures. Because this theory has been described and used in several publications, see e.g. [31–33], we write down only the final equations. The density profile equation, obtained by minimizing the excess grand canonical potential:

$$\begin{aligned}\Omega_{ex} = {} & \int \{\Phi[\rho_1(z), \rho_2(z)] - \Phi[\rho_{b1}, \rho_{b2}]\}\,\mathrm{d}\boldsymbol{r} - \sum_{i=1}^{2}\int \mathrm{d}\boldsymbol{r}\,\{\mu_i[\rho_i(z) - \rho_{bi}] - \rho_i(z)V(z)\} \\ & + \sum_{i=1}^{2}\int \mathrm{d}\boldsymbol{r}\,\{[\rho_i(z)\ln\rho_i(z) - \rho_i(z)] - [\rho_{bi}\ln\rho_{bi} - \rho_{bi}]\} \\ & + \tfrac{1}{2}\sum_{i,j=1}^{2}\int \mathrm{d}\boldsymbol{r}\int \mathrm{d}\boldsymbol{r}'[\rho_j(z')\rho_i(z) - \rho_{bj}\rho_{bi}]u_{ij}^{(att)}(|\boldsymbol{r} - \boldsymbol{r}'|),\end{aligned} \tag{4}$$

is

$$\begin{aligned}\ln[\rho_i(z)/\rho_{bi}] = {} & -\frac{1}{kT}\sum_{a=1}^{4}\int\left\{\frac{\partial\Phi}{\partial n_a(z')} - \left(\frac{\partial\Phi}{\partial n_a}\right)_{\{\rho(\boldsymbol{r}')=\rho_{bi}\}}\right\}w_a(|\boldsymbol{r} - \boldsymbol{r}'|)\,\mathrm{d}\boldsymbol{r}' \\ & - \frac{1}{kT}\sum_{a=1}^{2}\int\left\{\frac{\partial\Phi}{\partial \boldsymbol{n}_{va}(z')} - \left(\frac{\partial\Phi}{\partial \boldsymbol{n}_{va}}\right)_{\{\rho(\boldsymbol{r}')=\rho_{bi}\}}\right\}\boldsymbol{w}_a(|\boldsymbol{r} - \boldsymbol{r}'|)\,\mathrm{d}\boldsymbol{r}' - V(z)/kT \\ & + \sum_{j=1}^{2}\int \mathrm{d}\boldsymbol{r}'\,[\rho_j(z') - \rho_{bj}]u_{ij}^{(att)}(|\boldsymbol{r} - \boldsymbol{r}'|).\end{aligned} \tag{5}$$

In the above equation, μ_i is the configurational chemical potential of the component i, ρ_{bi} is the density of the ith component in a bulk fluid in equilibrium with the confined system, Φ is

the free energy functional of hard spheres [31–33],

$$\Phi/kT = -n_0 \ln(1-n_3) + \frac{n_1 n_2 - \boldsymbol{n}_{v1}\cdot\boldsymbol{n}_{v2}}{(1-n_3)} + \frac{n_2}{24\pi}\frac{[n_2^2 - \boldsymbol{n}_{v2}\cdot\boldsymbol{n}_{v2}]}{(1-n_3)^2} \tag{6}$$

and the quantities n_a and $\boldsymbol{n}_{va}$ are the averaged densities, given by the following equations:

$$n_a(z_1) = \sum_{i=1}^{2}\int \mathrm{d}\boldsymbol{r}_2\, \rho_i(z_2) w_a(r_{12}), \qquad a = 0, 1, 2, 3 \tag{7a}$$

$$\boldsymbol{n}_{va}(\boldsymbol{r}_1) = \sum_{i=1}^{2}\int \mathrm{d}\boldsymbol{r}_2\, \rho_i(\boldsymbol{r}_1+\boldsymbol{r}_2)\boldsymbol{w}_{va}(\boldsymbol{r}_2), \qquad a = 1, 2 \tag{7b}$$

where $w_a(r,\sigma)$, $a = 0, 1, 2, 3$ (scalar quantities) and $\boldsymbol{w}_{va}(\boldsymbol{r})$, $a = 1, 2$ (vector quantities) are the weight functions. The vectorial contribution to the free energy given by equation (6) is zero for a homogeneous fluid. Explicit expressions for the weight functions are given in [31, 32], Moreover, $u_{ij}^{(att)}(r)$ denotes the attractive part of the LJ potential (1), defined as common according to the Weeks–Chandler–Andersen scheme [34]:

$$u_{ij}^{(att)}(r) = \begin{cases} -\varepsilon_{ij}, & r < r_{ij,\min} \\ u_{ij}(r) & r \geqslant r_{ij,r\,\min}, \end{cases} \tag{8}$$

where $r_{ij,\min} = 2^{1/6}\sigma$. Moreover, the hard-sphere density functional has been evaluated assuming the hard-sphere diameters are equal to σ. The parameter σ is chosen as a unit of length in what follows.

The relationship between μ_i and ρ_{bi} is

$$\begin{aligned}\mu_i/kT = &-\ln(1-n_3) + (\sigma/2)n_2/(1-n_3) + (\sigma/2)^2[n_1/(1-n_3) + (1/8\pi)n_2^2/((1-n_3)^2)] \\ &+ (\sigma/2)^3[n_0/(1-n_3) + n_1 n_2/(1-n_3)^2 + (1/12\pi)n_2^3/(1-n_3)^3] \\ &+ \sum_{j=1,2}\rho_{bj}\int \mathrm{d}\boldsymbol{r}\, u_{ij}^{att}(r),\end{aligned} \tag{9}$$

where the average densities are calculated according to equation (7) with local densities equal to the bulk densities. We also introduce the symbol x to abbreviate the bulk fluid composition, $x = \rho_{b1}/\rho_b$, where $\rho_b = \rho_{b1} + \rho_{b2}$ is the total bulk fluid density. The dimensionless bulk density is ρ_b.

The method of solution of the density profile equation, equation (5), applied by us, is based on a standard iteration procedure. All the integrations have been carried out using Simpson's method with a grid size of 0.01σ.

The knowledge of the density profiles allows us to calculate the excess grand thermodynamic potential, Ω_{ex}, as well as the adsorption isotherm of species i, Γ_i, as functions of the chemical potentials of two components of the binary mixture in question:

$$\Gamma_i = \int_0^H \mathrm{d}z\, \rho_i(z). \tag{10}$$

The total isotherm is the sum of individual adsorptions, $\Gamma = \Gamma_1 + \Gamma_2$. We also define the average density in the pore, $\langle\rho\rangle = \Gamma/H$ and the selectivity, $S = \Gamma_1/\Gamma$. However, all the results presented below have been obtained for an *equimolar* bulk fluid composition, i.e. for $x = 0.5$. In other words the chemical potential of both species has been identical, $\mu_2 = \mu_1$, and thus $\beta\mu_1$ is the only independent variable. It will be denoted by $\beta\mu$ in what follows.

3. Results and discussion

First we would like to comment on the phase diagrams of the binary symmetric model mixtures considered in this work, i.e. M75, M65 and M55. Those phase diagrams serve as references for the further study of inhomogeneous fluids.

In each case the bulk phase diagram has been calculated according to the same procedure as that used for confined fluids (i.e. by minimizing Ω with respect to the total density of the mixture and to its composition, x, with external field switched off, however). In this work, we minimize Ω with respect to density at fixed equimolar composition. The T^*–ρ projections of the bulk phase diagrams for an equimolar composition of the gas phase are shown in figure 1. The λ-line of second-order transitions between mixed and demixed fluids is given by the dotted line in each panel. The position of that line, with respect to the envelope of the first-order transitions, mainly depends on the energy of the cross interaction. For the system with the highest energy of the cross interaction (model M75), the λ-line enters the coexistence envelope quite far below the liquid–vapour critical point. The critical end point (CEP) then appears. At the temperatures below the CEP a mixed vapour coexists with a demixed liquid. In the case of the strongest demixing, i.e. for model M55, the coexistence between a mixed vapour phase and demixed fluid terminates at a tricritical point. For an intermediate value of the cross interaction, i.e. for system M65, the phase diagram is characterized by the presence of a triple point and a tricritical point as well. A complete discussion of those three types of topology of the bulk phase diagrams can be found in the recent work by Wilding *et al* [21]. In all panels of figure 1 we have also included the lines representing the solutions leading to the metastable transitions between two different mixed phases, which are marked by chain curves.

We begin the discussion of nonuniform systems with the model fluid M75, confined to the pores of different width ($H = 5$ and 15) with attractive walls of moderate strength, $\varepsilon_{gs}/\varepsilon = 8$. The construction of the phase diagram requires the calculation of the isotherms and of the excess grand thermodynamic potential, Ω_{ex} (as functions of $\beta\mu_1$). The location of the first-order transition at each temperature is determined by the crossing point of two branches of Ω_{ex}, corresponding to the two coexisting phases. Some examples of the plots of $\beta\Omega_{ex}$ for the pore $H = 15$ are given in figure 2(a). The line with dark symbols corresponds to demixed states of the mixture. The corresponding adsorption isotherms are shown in figure 2(b). In general, the adsorption isotherms exhibit hysteresis. However, metastable parts of the isotherms have been discarded and only jumps resulting from the first-order transitions (capillary condensation of a mixture in the pore) are shown in figure 2(b). Two solutions of the equation for the density profiles describe two phases of different density and composition. An example of the changes of the density profiles upon the capillary condensation transition is shown in figure 3.

At the temperature, $T^* = 1.0$, the confined fluid also undergoes the second-order demixing transition, in addition to capillary condensation. The branch of $\beta\Omega_{ex}$ describing states with $S \neq 0.5$ is stable with respect to the branch for $S = 0.5$, see the line with symbols in figure 2(a). This transition occurs at the chemical potential higher than the bulk coexistence and hence the relevant curve in figure 2(a) is cut and consists of two disconnected parts. The corresponding part of the adsorption isotherm shows higher adsorption for the selectivity $S \neq 0.5$. It is important that the branches of the isotherm corresponding to $S \neq 0.5$ and $S = 0.5$ meet tangentially at the transition point of the λ-line.

The phase diagrams resulting from the analysis described above are displayed in figure 4, which also presents the bulk phase diagram as a reference. The narrowing of a pore results in shrinking the coexistence envelope and lowering the critical temperature of the capillary condensation and also lowering the CEP. However, the inclination of the λ-line remains practically unchanged for the two confined systems and the bulk.

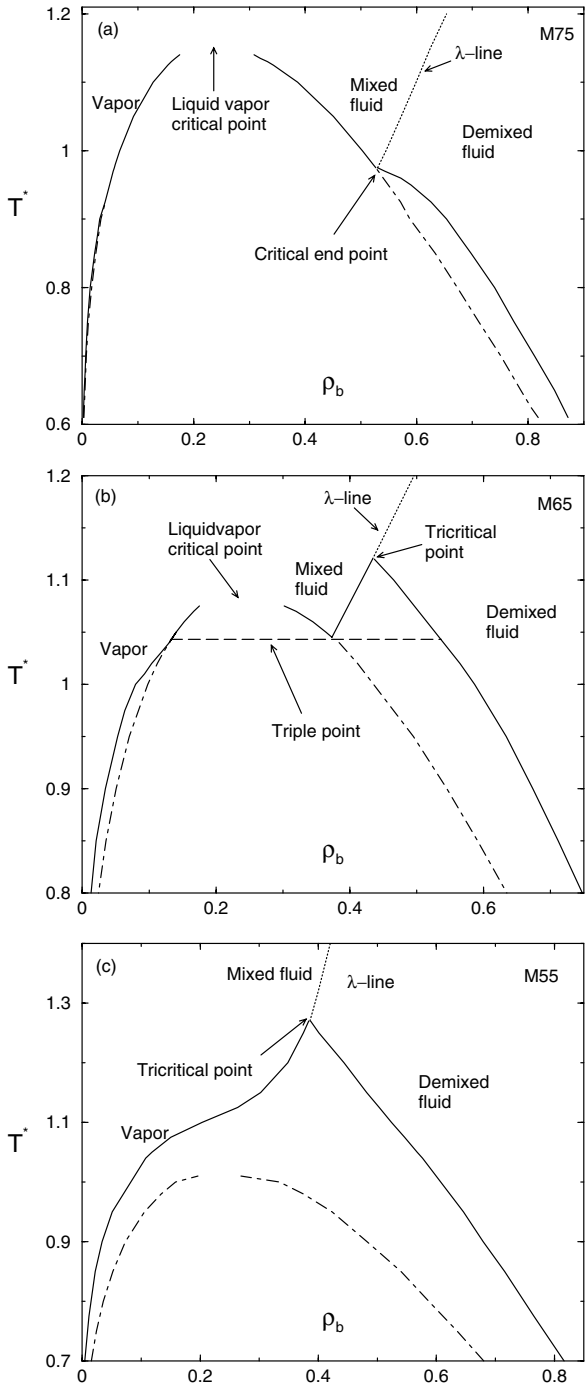

Figure 1. Bulk phase diagrams for three model systems investigated. The composition along the vapour branch is 0.5. Chain curves correspond to metastable states between two mixed phases.

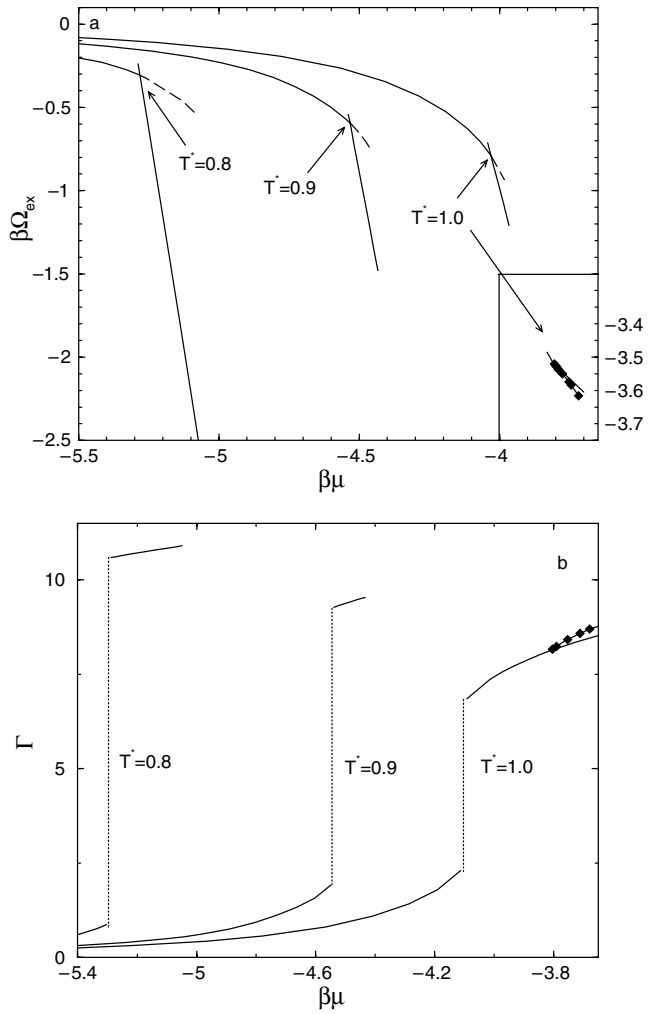

Figure 2. Illustration of the method of construction of the phase diagrams for confined systems. Part (a) shows the dependence of the excess grand potential on the configurational chemical potential and part (b) shows the adsorption isotherms. In the case of a first-order transition, the two branches of $\beta\Omega_{ex}$ intersect, while in the case of the second-order demixing transition, shown in the inset, they meet together tangentially. Note that the grand potential scale of the inset is changed. The calculations have been carried out for a M75 fluid in the pore of $H = 15$ and $\varepsilon_{gs} = 8$. Curves with symbols denote the values of $\beta\Omega_{ex}$ and Γ for a demixed confined fluid.

In the case of a stronger fluid–solid interaction, $\varepsilon_{gs} = 11$, the effects of the confinement are similar to those described above. However, a low density branch of the coexistence envelope shows a new feature at sufficiently low temperatures (figure 5(a)). For a wide pore of $H = 15$ one observes the first-order layering transition with a well defined critical point, while for a narrower pore of $H = 5$, only a non-monotonic change of the coexistence line is a remnant of that transition. Also, the transition between mixed and demixed phases shifts slightly to a higher density as the pore becomes narrower. Capillary condensation occurs at chemical potential values below the bulk coexistence, see figure 5(b). This figure also shows that the layering transition is present for the pore $H = 15$ and persists for a pore of $H = 10$. The

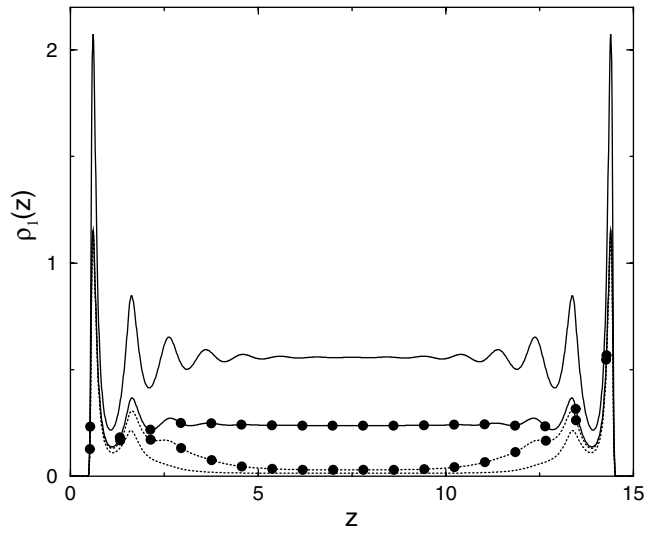

Figure 3. The equilibrium density profile for component 1, $\rho_1(z)$, for coexisting phases in the pore of $H = 15$ and $\varepsilon_{gs} = 8$ at $T^* = 0.9$ (curves) and $T^* = 1.0$ (curves with full circles). Full and broken curves are the profiles after and before the capillary condensation, respectively.

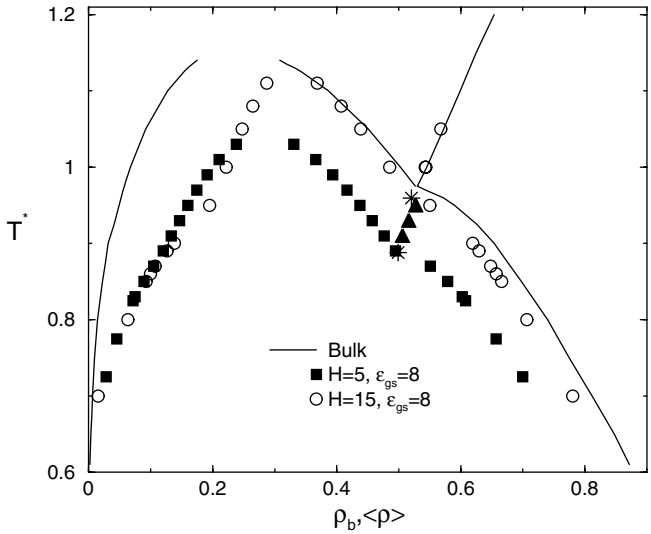

Figure 4. A comparison of the phase diagrams for model M75 in a slit-like pore of the width $H = 15$ (empty symbols) and $H = 5$ (full symbols) and in the bulk (curves). The adsorption potential is characterized by $\varepsilon_{gs} = 8$. Asterisks indicate the CEPs.

layering transitions are the features characteristic for adsorption at a single wall and thus they become suppressed in sufficiently narrow pores. The second-order demixing transition occurs practically at the same values of the chemical potential for both the bulk and confined systems.

The increase of the adsorption energy, up to $\varepsilon_{gs} = 15$, introduces qualitatively new features to the phase behaviour of the confined M75 fluid (see figures 6(a) and (b)). In particular, for both pores of $H = 10$ and 15 the demixing lines start at the low density side of the coexistence curve

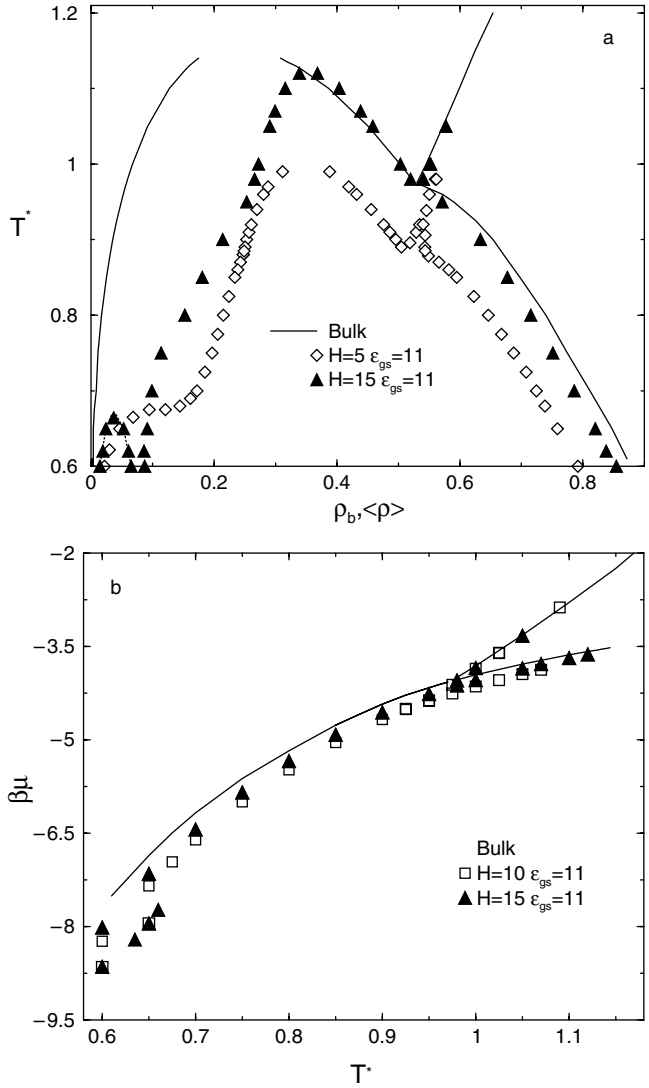

Figure 5. Part (a) the T^*–ρ projection, and part (b) the T^*–$\beta\mu$ projection of the phase diagram for the fluid M75 in the pores (symbols) and in the bulk (curves). The adsorption potential is characterized by $\varepsilon_{gs} = 11$. The nomenclature of the symbols is given in the figure.

and enter the following parts of the phase diagram, corresponding to the layering transition and capillary condensation. Those lines meet the first-order coexistence at the CEPs marked by the asterisks. The difference between the pores of $H = 10$ and 15 results from the changes in the low density parts of the phase diagrams, associated with the layering transitions and with the locations of the triple points. The position of the low density part of the λ-line shifts when the pore width changes substantially, while the high density part of that line remains almost unchanged. The selectivity changes along the phase boundaries of demixed phases for the case of $H = 15$ are shown in figure 6(c) where each branch terminates at equimolar selectivity. The labels for the terminating points in this figure coincide with those given in figure 6(b).

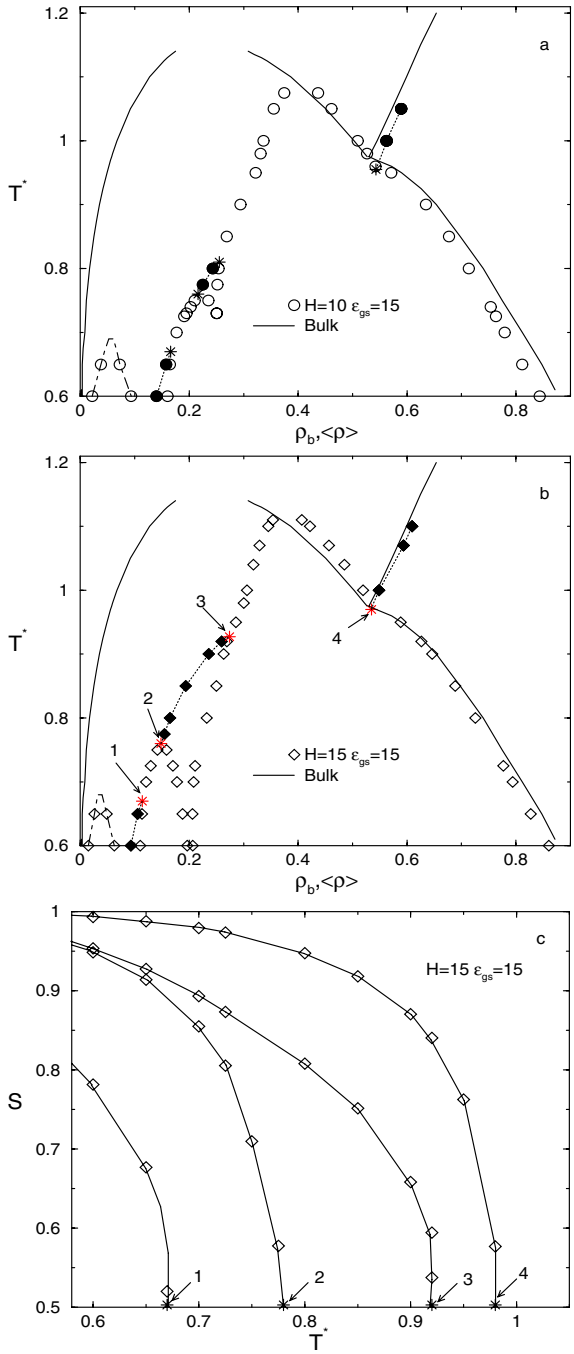

Figure 6. Parts (a) and (b): the T^*–ρ projections, and (c): the T^*–S projection of the phase diagrams for the fluid M75 in the pores (symbols) and in the bulk (curves). The adsorption potential is characterized by $\varepsilon_{gs} = 15$. The nomenclature of the symbols is given in the figure. The white and dark symbols refer to the first-order transitions and λ-line, respectively. Asterisks indicate the CEPs, which are labelled in parts (b) and (c) with the numbers 1, 2, 3 and 4.

(This figure is in colour only in the electronic version)

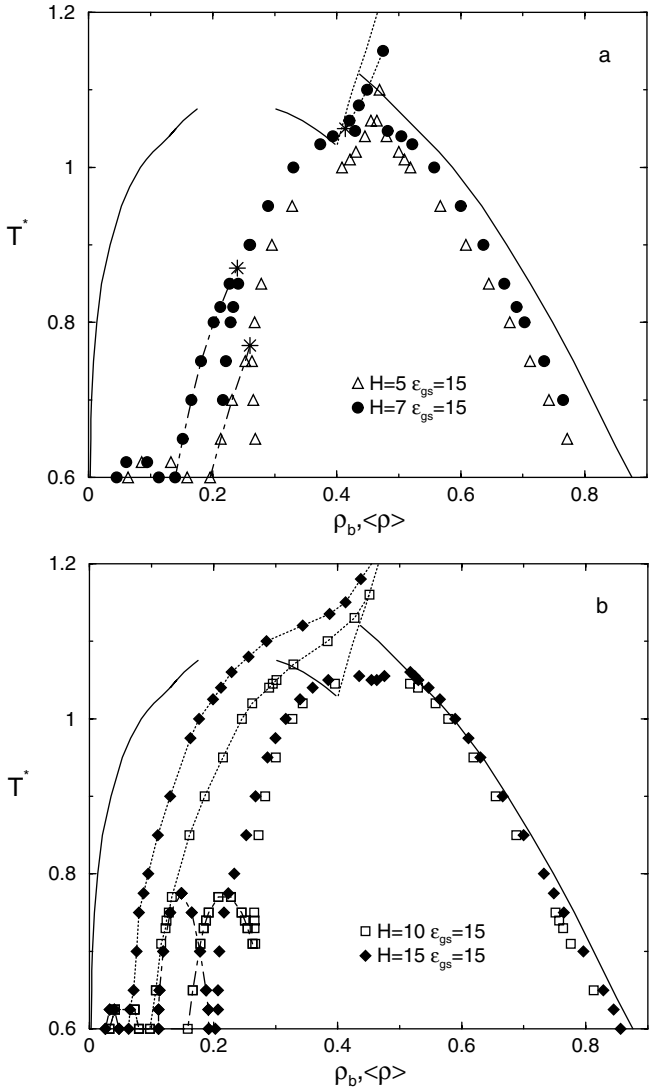

Figure 7. The T^*–ρ projections of the phase diagrams for the fluid M65 in the pores (symbols) and in the bulk (curves). Parts (a) and (b) are for different pore widths, indicated in the figure. The adsorption potential is characterized by $\varepsilon_{gs} = 15$. The nomenclature of the symbols is given in the figure. Asterisks indicate the CEPs.

The next figures, figures 7(a) and (b), demonstrate the phase diagrams for model M65 confined in pores with strongly attractive walls ($\varepsilon_{gs} = 15$) of different widths. This model is characterized by stronger demixing, in comparison to model M75, and consequently the multiplicity of the CEPs of the λ-line is observed for narrow pores only, $H = 5$ and 7. In particular, in the case of $H = 7$ the upper CEP almost coincides with the critical temperature. For even narrower pores, the type of phase diagram changes from the second to the third class [21], characterized by the absence of a critical point and the presence of the tricritical point. However, for wider pores ($H = 10$ and 15) the demixing line is continuous and entirely separated from the coexistence envelopes for the first-order transitions, within the temperature

range investigated. Concerning the λ lines and capillary condensation the type of topology of the phase diagrams has not been observed for the bulk models.

The first-order first layering transitions are observed for all cases in question. For wider pores the second layering transition exists as well. For the widest pore studied, the upper part of the capillary condensation envelope for the coexistence between demixed phases weakly splits into two branches. This implicitly shows that condensation occurs in two stages. The first stage is the layering transition involving condensation within the third and fourth layer simultaneously, while the second results from the filling of the remaining part of the pore.

The last part of our study has been carried out for model M55. This fluid exhibits the strongest demixing and its bulk phase diagram belongs to the third class. Figure 8 shows examples of the phase diagrams obtained for pores of the width $H = 10$ and 20 and of different strength of the fluid–solid interaction. For sufficiently low values of ε_{gs}, $\varepsilon_{gs} = 5$, the phase diagrams for the confined fluid are topologically the same as for the bulk. The envelopes end at the tricritical points whose temperatures decrease very slightly with the decrease of the pore width. On the other hand, when the fluid–wall interaction energy becomes sufficiently strong, $\varepsilon_{gs} = 15$ (cf figure 8(b)) the topology of the phase diagrams changes. There appears a sequence of first-order layering transitions. The λ-line starts at the tricritical point of the first layering transition and is completely separated from the other parts of the phase diagram. As a consequence the capillary condensation transition terminates at a critical point, rather than at the tricritical point characteristic for the bulk and for the pores with weakly adsorbing walls. The identification of the particular phases in figure 8(b) is not trivial and requires a careful inspection of the density profiles and thermodynamic quantities. Figures 9 and 10 give just an example of such an analysis. The results presented here have been obtained for $H = 10$ and at $T^* = 0.7$ (i.e. very slightly above the triple point temperature between the second layering transition and the capillary condensation). Figure 9 presents a part of the adsorption isotherm, which shows the second layering transition and the capillary condensation, and the corresponding excess grand canonical potential. Figures 10(a) and (b) illustrate the changes in the structure of the confined fluid. Full and dotted curves are the profiles evaluated at the chemical potential just below and above the second layering transition, respectively, whereas the broken lines represent the condensed fluid filling the entire pore. Note that the amount of the second component (figure 10(b)) in that condensed phase is considerably lower than the amount of the first component (figure 10(a)).

4. Conclusions

We have investigated the adsorption of symmetric binary mixtures, which exhibit three types of bulk phase behaviour. Our observations regarding the types of the phase behaviour are the following. In the case of *weak* fluid–solid interactions the phase diagrams can exhibit:

(1) Mixed gas to mixed liquid first-order transition at higher temperatures, that terminates at the critical point and mixed gas to demixed liquid first-order transition at lower temperatures. There exists a triple point temperature, separating the above two regimes. This type of behaviour can be observed in narrow and wide pores.
(2) The first-order transition between two mixed phases disappears and the corresponding triple point disappears. We have the first-order transition between mixed gas and demixed denser fluid with a tricritical point. Such phase behaviour exists in narrow, as well as in wider, pores, dependent on the value of adsorption energy.

In the case of *strong* fluid–solid interactions we have found:

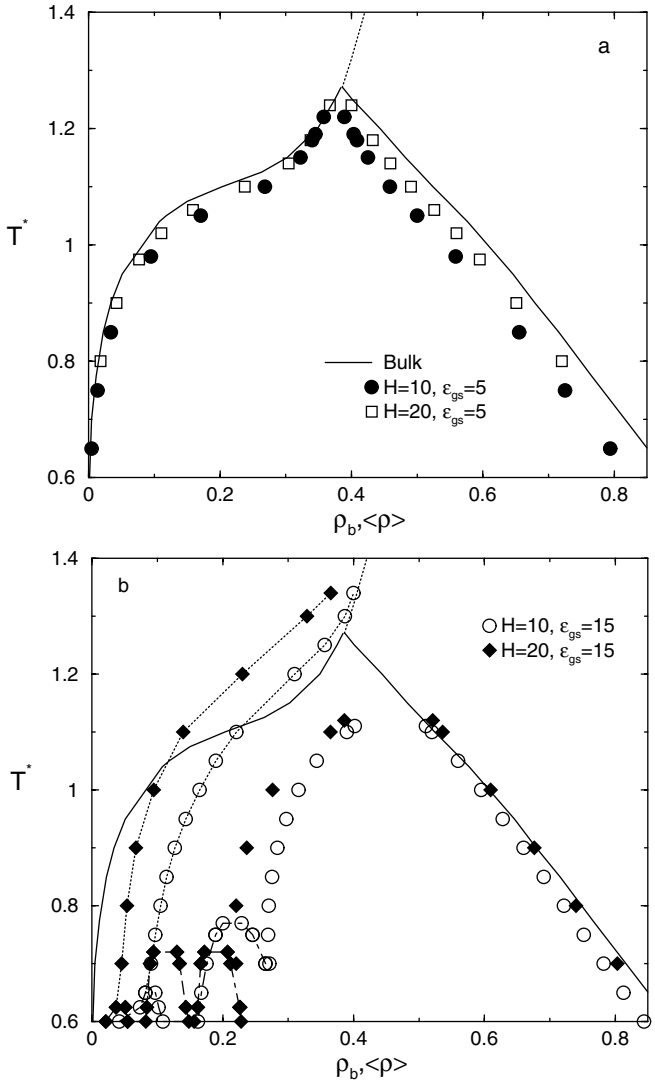

Figure 8. The T^*–ρ projections of the phase diagrams for the fluid M55 in the pores (symbols) and in the bulk (curves). Parts (a) and (b) are for different pores, indicated in the figure. The nomenclature of the symbols is given in the figure.

(1) In addition to capillary condensation, layering phase transitions between either mixed–mixed, mixed–demixed or demixed–demixed, two phases of relatively low average densities can be found at low temperatures.
(2) The λ-type line can join the first-order transitions (layering or capillary condensation) at CEPs. Multiplicity of the CEPs has been observed for the first time.
(3) The λ-line can decouple from the capillary condensation part of the phase diagram for sufficiently wide pores.

Assessing the significance of the above results one should remember that they have been obtained within the density functional theory that is based on a mean field approximation.

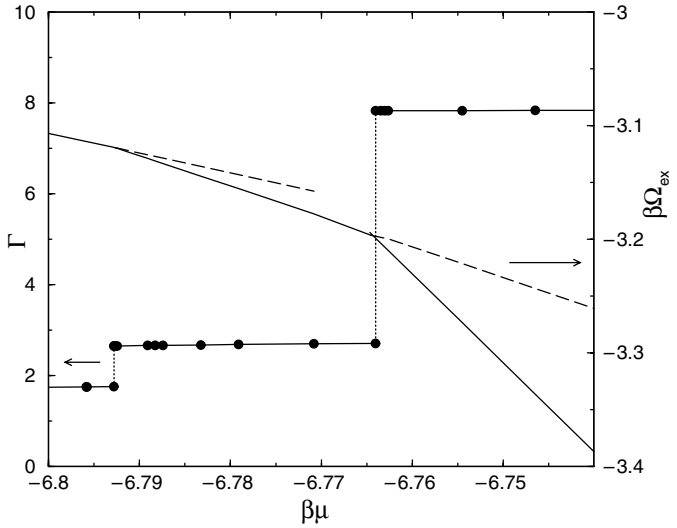

Figure 9. Examples of the adsorption isotherm and of the excess grand potential at $T^* = 0.7$, $\varepsilon_{gs} = 15$ and for $H = 10$. This temperature is marginally higher than the triple point temperature between the second layering transition and the capillary condensation, see figure 8(b). Broken lines for $\beta\Omega_{ex}$ correspond to mixed phases which are metastable with respect to demixed phases (full lines).

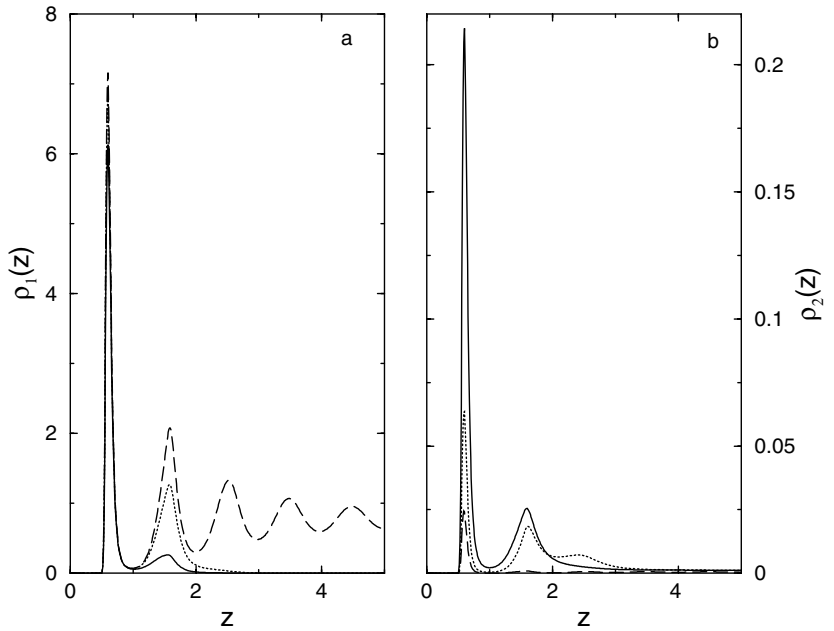

Figure 10. The density profiles, $\rho_i(z)$, of species 1 (part (a)) and 2 (part (b)) for coexisting phases at the transition points shown in figure 9. Full and dotted curves are the profiles just before and after the second layering transition, respectively. Broken curves are the profiles after the capillary condensation.

Other types of phase behaviour are possible as well even for the model mixtures considered in this work. In particular, we have not included the possible influence of wetting on the phase behaviour of a fluid confined in a pore. In particular, we have not explored the possible interplay relation between wetting properties of a single wall and phase behaviour of the same fluid mixture in narrow pores, which can be established by considering very wide pores and performing systematic changes of the interaction energy between solid walls and fluid components. Here we only state that, in the case of weakly adsorbing walls, the phase diagrams plotted in the selectivity–temperature plane are similar for all investigated pores. In this case, the effect of the confinement is quite usual and a decrease of the pore width causes the shift of the entire phase diagram down the temperature axis. However, for higher adsorbing potentials the phase diagram can be changed.

Acknowledgments

This work has been supported by KBN of Poland under grant no 3T09AAdsMix, by the CONACyT of Mexico under grant 37323-E and by the National University of Mexico under grant IN-113201.

References

[1] Gelb L D, Gubbins K E, Radhakrishnan R and Śliwinska-Bartkowiak M 1999 *Rep. Prog. Phys.* **62** 1572
[2] Dietrich S and Schick M 1986 *Phys. Rev.* B **33** 4952
[3] Grabowski K, Patrykiejew A and Sokołowski S 1997 *Thin Solid Films* **304** 344
Grabowski K, Patrykiejew A and Sokołowski S 1999 *Thin Solid Films* **342** 259
[4] Śliwinska-Bartkowiak M, Sowers S L and Gubbins K E 1996 *Langmuir* **13** 1182
[5] Choudhury N and Ghosh S K 2001 *Phys. Rev.* E **64** 021206
[6] Schmid F and Wilding N B 2001 *Phys. Rev.* E **63** 031201
[7] Tovbin Y K, Zhidkova L K and Komarov V N 2001 *Russ. J. Chem.* B **50** 786
[8] Shevade A V, Jiang S and Gubbins K E 2000 *J. Chem. Phys.* **113** 6933
[9] Bulnes F, Ramirez-Pastor A J and Pereyra V D 2001 *J. Mol. Catal. A: Chem.* **167** 129
[10] Cracknell R F, Nicholson D and Quirke N 1993 *Mol. Phys.* **80** 885
[11] Heffelfinger G S, Tan Z, Gubbins K E, Marconi U M B and van Swol F 1989 *Mol. Simul.* **2** 393
[12] Heffelfinger G S, van Swol F and Gubbins K E 1988 *J. Chem. Phys.* **89** 5202
[13] Jiang S, Gubbins K E and Balbuena P B 1994 *J. Phys. Chem.* **98** 2403
[14] Góźdź W T, Gubbins K E and Panagiotopoulos A Z 1995 *Mol. Phys.* **84** 825
[15] Sokołowski S and Fischer J 1990 *Mol. Phys.* **71** 393
[16] Tan Z and Gubbins K E 1992 *J. Phys. Chem.* **96** 845
[17] Rowlinson J S and Swinton F L 1982 *Liquids and Liquid Mixtures* (London: Butterworths)
[18] Vidales A, Benavides A L and Gil-Villegas A 2001 *Mol. Phys.* **99** 703
[19] Wang Ji-Lin, Wu Guang-Wen and Sadus R J 2000 *Mol. Phys.* **98** 715
[20] Kahl G, Schöll-Paschinger E and Lang A 2001 *Monatsch. Chem.* **132** 1413
[21] Wilding N B, Schmid F and Nielaba P 1998 *Phys. Rev.* E **58** 2201
[22] van Konynenburg P H and Scott R L 1980 *Phil. Trans. R. Soc.* A **298** 495
[23] Patrykiejew A, Reszko-Zygmunt J, Sokołowski S and Sokołowska Z 2003 *Mol. Phys.* at press
[24] Schöll-Paschinger E, Levesque D, Weis J J and Kahl G 2001 *Phys. Rev.* E **64** 011502
[25] Paschinger E and Kahl G 2000 *Phys. Rev.* E **61** 5330
[26] Gordon P A and Glandt E D 1996 *J. Chem. Phys.* **105** 4257
[27] Tremblay L, Socol S M and Lacelle S 2000 *Phys. Rev.* E **61** 656
[28] Wendland M 1998 *Fluid Phase Equilib.* **147** 105
[29] Stecki J and Toxvaerd S 1995 *J. Chem. Phys.* **102** 7163
Stecki J and Toxvaerd S 1995 *J. Chem. Phys.* **103** 4352
Stecki J and Toxvaerd S 1995 *J. Chem. Phys.* **103** 9763
[30] Iatsevitch S and Forstmann F 2001 *J. Phys.: Condens. Matter* **13** 4769
[31] Rosenfeld Y 1989 *Phys. Rev. Lett.* **63** 980
[32] Roth S and Dietrich S 2000 *Phys. Rev.* E **62** 6926
[33] Schmidt M 2000 *Phys. Rev.* E **62** 3799
[34] Weeks J D, Chandler D and Andersen H C 1971 *J. Chem. Phys.* **54** 5237